AGU PUBLICATIONS

JGR

Journal of Geophysical Research: Space Physics

RESEARCH ARTICLE

10.1002/2016JA023018

Key Points:

- The magnetosphere responds to a change in IMF B_y in less than 15 min in all local times from the presumed arrival at the bow shock
- At geosynchronous distances, the reconfiguration time is less than 45 min in all local time sectors
- The reconfiguration time and magnitude of the induced B_y component depend on the solar wind velocity

Correspondence to:
P. Tenfjord,
paul.tenfjord@uib.no

Citation:
Tenfjord, P., N. Østgaard, R. Strangeway, S. Haaland, K. Snekvik, K. M. Laundal, J. P. Reistad, and S. E. Milan (2016), Magnetospheric response and reconfiguration times following IMF B_y reversals, *J. Geophys. Res. Space Physics*, *122*, doi:10.1002/2016JA023018.

Received 2 JUN 2016
Accepted 29 NOV 2016
Accepted article online 22 DEC 2016

Magnetospheric response and reconfiguration times following IMF B_y reversals

P. Tenfjord[1], N. Østgaard[1], R. Strangeway[2], S. Haaland[1,3], K. Snekvik[1], K. M. Laundal[1], J. P. Reistad[1], and S. E. Milan[1,4]

[1]Birkeland Centre for Space Science, Department of Physics and Technology, University of Bergen, Bergen, Norway, [2]Institute of Geophysics and Planetary Physics, University of California, Los Angeles, California, USA, [3]Department of Physics and Astronomy, University of Leicester, Leicester, UK, [4]Max Planck Institute for Solar System Research, Göttingen, Germany

Abstract The interaction between the interplanetary magnetic field (IMF) and the geomagnetic field at the dayside magnetopause leads to transfer of momentum and energy which changes the magnetospheric configuration, but only after a certain time. In this study we quantify this time, to advance our understanding of the causes for the delayed response of the magnetosphere. We study the response and reconfiguration time of the inner magnetosphere to IMF B_y reversals. A superposed epoch analysis of magnetic field measurements from four Geostationary Operational Environmental Satellite spacecraft at different local times both for negative to positive IMF B_y reversals and for positive to negative reversals is presented. The magnetospheric response time at geosynchronous orbit to the sudden change of IMF B_y is less than 15 (∼10) min from the bow shock (magnetopause) arrival time, while the reconfiguration time is less than 46 (∼41) min. These results are consistent with a B_y component induced on closed magnetic field lines due to the asymmetric loading of flux following asymmetric dayside reconnection when IMF $B_y \neq 0$. Our results also confirm our earlier studies that nightside reconnection is not required for generating a B_y component on closed field lines.

1. Introduction

Abrupt changes in the solar wind and interplanetary magnetic field lead to changes in the magnetosphere and ionosphere, but only after a certain time. In this study we focus on the impact of the interplanetary magnetic field (IMF) B_y component on the magnetospheric dynamics at geosynchronous distances. The IMF B_y induces a B_y component in the closed magnetosphere through asymmetric loading of flux to the lobes, resulting from dayside reconnection. We study the temporal evolution of the resulting asymmetric stresses. When these stresses are communicated to the different regions of the closed magnetosphere, we observe an induced B_y component. This mechanism is explained in detail in *Tenfjord et al.* [2015], where the response to a sudden change in IMF B_y was simulated using the Lyon-Fedder-Mobarry magnetohydrodynamics (MHD) model [*Lyon et al.*, 2004]. Based on the MHD simulation results and theoretical considerations, *Tenfjord et al.* [2015] suggested that the time to induce a B_y component in the closed magnetosphere should be of the order of tens of minutes. This study is a follow-up study to explore whether the predicted timing is supported by observations.

The time it takes for the ionosphere to respond (initial onset) and reconfigure (time scale to reach final configuration) to a change in the solar wind conditions has been studied using a variety of techniques, ranging from ground-based and spacecraft instruments to numerical modeling [e.g., *Nishida*, 1968; *Friis-Christensen et al.*, 1985; *Ridley and Clauer*, 1996; *Dudeney et al.*, 1998; *Khan and Cowley*, 1999; *Lu et al.*, 2002; *Ruohoniemi et al.*, 2002; *Kabin et al.*, 2003; *Merkin et al.*, 2013]. Using Super Dual Auroral Radar Network global convection patterns, *Grocott and Milan* [2014] inferred that after a change in the IMF clock angle, during southward IMF B_z, the magnetosphere reaches an equilibrium state within 20–30 min. *Kabin et al.* [2003] studied the response and reconfiguration time during IMF B_y reversals using an MHD model. The authors found that the ionospheric convection responded after 4–8 min and took 15–20 min to reconfigure. *Yu and Ridley* [2009] analyzed the effect of a sudden change in IMF B_z using the Block-Adaptive-Tree-Solarwind-Roe-Upwind-Scheme (BATS-R-US) MHD model. Their results agree well with the result from *Kabin et al.* [2003]. *Wing et al.* [2002] analyzed the time-dependent response of the magnetic field at geosynchronous orbit to sudden changes in IMF

B_z orientation using Geostationary Operational Environmental Satellite (GOES). They found the response at all local times on the dayside to be 4–5 min and the nightside response time to be 12 min.

There are several processes that can contribute to the observed B_y component in the closed magnetosphere. The physical mechanisms responsible for inducing a B_y component are usually not specified. Instead, the term "IMF B_y penetration" is used. This term is used as a very generic and broad term and includes all the different physical mechanisms actually responsible for generating a magnetospheric B_y component [*Petrukovich*, 2009, 2011]. As suggested by *Tenfjord et al.* [2015], we use the term "induced" and specify the agent or process responsible for producing a B_y component in the closed magnetosphere.

Using 9 years of Cluster data, *Cao et al.* [2014] studied how the "penetration" of IMF B_y in the neutral sheet depends upon IMF B_z and the *Kp* index. The authors did not consider the time delay of the response of magnetosphere to solar wind parameters. Using global auroral imaging, *Østgaard et al.* [2011] found that asymmetric magnetic field foot points (measured as ΔMLT), which is a signature of an induced B_y, between the two hemispheres were established after only about 10 min. However, they did not recognize that this time delay is inconsistent with their interpretation of reconnection being responsible for this, since the tail reconnection occurs on considerably longer time scales (∼1 h).

Rong et al. [2015] reported the penetration of IMF into the magnetotail to be delayed by 1–1.5 h, based on two events. *Motoba et al.* [2011] analyzed one event and found the highest correlation between IMF B_y and B_y in the central magnetotail measured by Cluster when lagging the solar wind by 51 (57 from bow shock reference) min (reconfiguration time defined by maximum correlation). These results will be discussed in section 5.

Another example of timing is given by *Fear and Milan* [2012], where the authors showed the delay of the IMF B_y dependence on the magnetic local time at which transpolar arcs form to be as long as 3–4 h. Transpolar arcs occur predominantly when the IMF has a northward component, and the physical mechanism responsible for generating B_y during such conditions could be different compared to southward IMF. However, we will only discuss how the B_y component is induced during IMF $B_z < 0$ conditions.

In this study we perform an analysis of multispacecraft (GOES 8, GOES 10, GOES 11, GOES 12, and solar wind monitors) data to study the response and reconfiguration at different local times at geosynchronous orbit following sudden changes of the IMF B_y component for events favoring dayside reconnection.

The outline of the paper is as follows: In section 2 we describe how B_y in the magnetosphere is induced through dayside reconnection and asymmetric loading of magnetic flux. Section 3 describes the data used, the criteria applied to favor the IMF-induced B_y conditions, and an example of the methodology. In section 4 we present a superposed epoch analysis between the IMF B_y reversals and magnetic field measurements from four GOES spacecraft in the dayside and nightside. In section 5 we discuss the timing results and investigate the effects of other mechanisms able to induce B_y in the magnetosphere. We also discuss our results in the context of earlier studies of this topic. Concluding remarks are given in section 6.

2. Theory

The response time is here defined as the time between the change of IMF B_y at the bow shock and the onset of a change in the local (internal) field. We define reconfiguration time as the time it takes to reach the final configuration of a new state, with error bars based on uncertainty in data. We use the 1 min OMNI solar wind data, time shifted to the Earth's bow shock, to time tag IMF B_y changes. All times given are relative to this bow shock reference time. Note that there is an additional 4–8 min for the IMF phase fronts to propagate from the bow shock to the dayside magnetopause [*Slinker et al.*, 1998; *Kabin et al.*, 2003].

Dayside reconnection with an IMF B_y component results in asymmetric loading of flux in the lobes. For a positive IMF B_y, newly reconnected field lines on the dayside in the Northern Hemisphere will be deflected dawnward by magnetic tension. This asymmetric loading of magnetic flux creates a region of enhanced magnetic pressure in the northern dawn and southern dusk lobes. The enhanced pressure would propagate as a fast mode wave across the field lines from the lobes to the inner magnetosphere. This excites *y* directed shear flows in both the dayside and nightside magnetosphere. These flows are directed in opposite directions in the two hemispheres. Following this idea, first suggested by *Khurana et al.* [1996], and adapted by *Liou and Newell* [2010], *Tenfjord et al.* [2015] argued that these flows also affect closed field lines already present in the magnetosphere and therefore induce a B_y component on closed field lines.

An alternative mechanism is that a B_y component on closed field lines follows from nightside reconnection of field lines with nonconjugate foot points [*Cowley*, 1981; *Hau and Erickson*, 1995; *Stenbaek-Nielsen and Otto*, 1997; *Østgaard et al.*, 2004]. In this scenario, the response on closed field lines is expected to be considerably slower compared to the more "direct" shear flows inducing B_y and asymmetric foot points. This differs from the mechanism explained in *Tenfjord et al.* [2015] in that it relies on tail reconnection in order to produce B_y on closed field lines.

In a MHD description, the time scales of large-scale dynamics depend on the Alfvén velocity. Magnetic energy is converted into plasma motion only with the passage of an Alfvén wave, and the conversion is progressive rather than explosive [*Parker*, 2007]. We therefore expect a response time, depending on the propagation of the compressional Alfvén wave, responding to a change in the distribution of magnetic flux. The gradual buildup of magnetic pressure in the lobes results in a gradual reconfiguration [e.g., *Caan et al.*, 1975]. Although there are variations in the empirical studies of the ionospheric response time, results largely agree that the response takes less than 15 min while the reconfiguration takes less than 40 min [*Kabin et al.*, 2003, and references therein]. We will show that our results corroborate these results also for the induced B_y component.

2.1. Sources of B_y in the Magnetosphere

The term induced implies a perturbation of the existing background field by an external process. An induced B_y component in the closed magnetosphere can be generated by several processes, which may either counteract or enhance each other. The perturbations can also be more or less pronounced depending on location.

Magnetospheric B_y perturbations can be caused by any combination of the following mechanisms:

1. *IMF-induced B_y*: asymmetric loading of magnetic flux in the lobes [*Tenfjord et al.*, 2015]. This is illustrated in Figure 1a, looking from the magnetotail toward the Sun for a positive IMF B_y. Asymmetric reconnection leads to asymmetric loading of flux to the northern dawn and southern dusk lobes and results in asymmetric plasma flow (thick arrows) between the northern and southern lobes. This mechanism is the focus of the present paper. We have by design chosen conditions that favor asymmetric loading of flux to the lobes via dayside reconnection while trying to suppress influences from the other mechanisms listed below. The criteria to achieve this are listed in section 3.3.
2. *Twist-induced B_y*: a direct result of the asymmetric loading of flux to the lobes. Pressure balance between the lobes causes the entire tail, including the neutral sheet, to rotate around the tail axis [*Cowley*, 1981]. If one assumes that the magnetic field follows rotation of the normal to the twisted neutral sheet, the B_y component inside the magnetosphere will be oppositely directed to the IMF B_y and thus represents a damping of the IMF-induced B_y. In models, the contribution to B_y in our region of interest has been shown to be small [see *Petrukovich*, 2009; *Tsyganenko and Fairfield*, 2004], but the effect becomes more pronounced farther tailward [e.g., *Walker et al.*, 1999; *Kullen and Janhunen*, 2004]. At geosynchronous distances, the contribution from this process is negligible.
3. *Tilt-induced B_y*: The seasonal and diurnal tilting of the plasma sheet in the *XZ* plane results in a warping of the current sheet in the *YZ* plane, as seen in Figure 1b. To our knowledge, this is the second most important mechanism and may even dominate over IMF-induced B_y modulations in certain regions and for large tilt angles. The shape of the current sheet also depends on the solar wind pressure and strength and direction of IMF B_z [e.g., *Tsyganenko and Fairfield*, 2004].
   When flux is added asymmetrically (resulting in an IMF-induced B_y) during periods with large tilt angle, the warped current sheet is no longer symmetric with respect to the noon-midnight meridian. The current sheet is then forced to a configuration which is a combination of the twisting (Figure 1a) of the current sheet and the warping (Figure 1b), making the final configuration skewed.
4. *Dipolarization-induced B_y* on the nightside: Substorms and bursty bulk flows are associated with earthward propagating dipolarization fronts [e.g., *Angelopoulos et al.*, 1992]. Magnetic and plasma pressure enhance in the region of the return flow, before the region of dipolarization expands azimuthally. The azimuthal expansion of the return flow near Earth deforms the magnetic field, resulting in the region 2 Birkeland current system [e.g., *Parker*, 1996; *Snekvik et al.*, 2007]. These signatures are observed at GOES at times with high substorm activity. In section 3.3 we discuss how to suppress the contribution from this effect.

Petrukovich [2011] lists magnetotail flaring (in the *XY* plane) as the second most important source for the observed B_y. The flaring increases from the noon-midnight meridian toward the flanks. This B_y component exists simply due to the confinement of the magnetosphere by the constant external stresses applied by

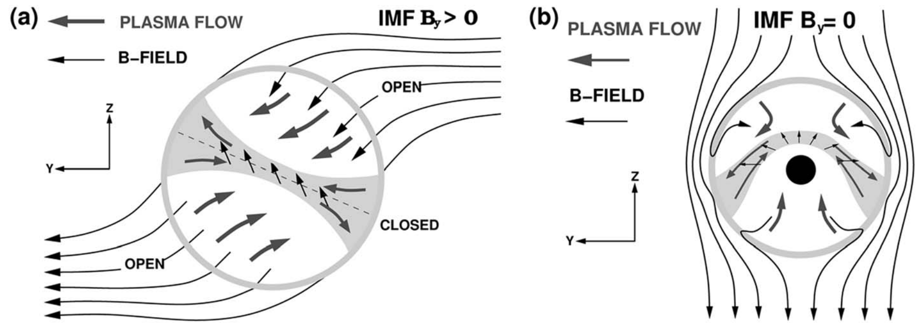

Figure 1. A schematic diagram of cross-sectional view of tilted magnetotail fields in the plasma sheet associated (a) with a positive IMF B_y field and (b) with a positive dipole tilt (northern summer). The geocentric solar magnetospheric coordinate system is used, and the view is from the tail toward the Earth. Figure is from *Liou and Newell* [2010].

the magnetosheath flow on the magnetopause, compressing the dayside and stretching the magnetotail. We regard this as a part of the background field and assume that at geosynchronous distances it is properly modeled by the Tsyganenko model (TS01) [*Tsyganenko*, 2002]. The question is, instead, how the closed field lines on the flanks are affected by other sources. We try to suppress the effect of the above processes in our statistical analysis by only including events where the effects of other mechanisms are small, by applying the criteria listed in section 3.3. In event studies, separating all these sources is nontrivial.

Petrukovich [2011] observed significant difference between premidnight and postmidnight and showed that the tilt-induced B_y component is also affected. No single mechanism is known to be responsible for this effect.

3. Data and Methodology

Below we present a superposed epoch analysis of GOES B_y magnetic field measurements and OMNI solar wind data from 1997 to 2013. Magnetic field measurements at geosynchronous orbit are obtained from the fluxgate instruments on GOES 8, GOES 10, GOES 11, and GOES 12 [*Singer et al.*, 1996]. The full constellation of spacecraft will henceforth be referred to as GOES only. The GOES orbit in solar magnetic (SM) coordinates (used throughout the paper) is shown in Figure 2. The background magnetic field (given in SM coordinates) shown in Figure 2 has been calculated using TS01 model when the dipole tilt angle was −28° (winter in Northern Hemisphere).

The OMNI solar wind data set is an extensive compilation of near-Earth spacecraft and plasma parameters [*King and Papitashvili*, 2005]. The 1 min OMNI solar wind magnetic field and plasma data have been time shifted to the Earth's bow shock nose by assuming continuously varying planar solar wind phase fronts convecting with the solar wind [*Haaland et al.*, 2006; *Weimer and King*, 2008; *Jackel et al.*, 2012]. Both OMNI and GOES 1 min data were obtained through http://cdaweb.gsfc.nasa.gov.

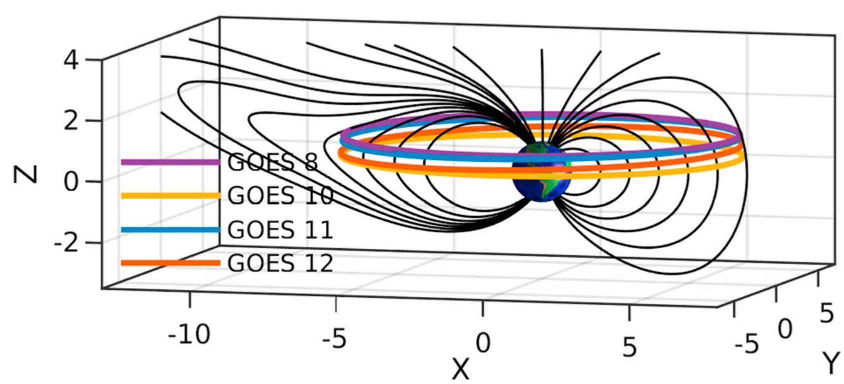

Figure 2. Orbit of GOES 8, GOES 10, GOES 11, and GOES 12 in SM coordinates, at $Z_{SM} \sim 1.2$, 0.51, 0.98, and 1.15 R_E northward of the geomagnetic equator, respectively. Background magnetic field lines (in SM coordinates) calculated using TS01 for IMF $B_z = -5$ nT, $B_y = 0$ nT, dynamic pressure $P_f = 10$ nPa, and $V_{SW} = 400$ km/s with dipole tilt angle of −28° (winter in Northern Hemisphere).

3.1. GOES Tilt Bias

GOES has a fixed geographic coordinates (GEO) location centered above North America. The foot points of the GOES spacecraft align roughly with both the geographical North Pole and the magnetic pole; that is, they are roughly along the same longitudinal meridian. Therefore, the 11.5° offset between the axis of rotation and the magnetic pole will be fixed with respect to the GOES foot point and Earth's rotation. This means that the GOES spacecraft always will be located northward of the magnetic equator ($Z_{sm} > 0$); see Figure 2. When the GOES foot point is sunward of the magnetic pole (close to noon), the diurnal tilt effect corresponds to +10° tilt independently of the axial tilt. Thus, a dipole tilt bias exists in the data. The orbital dynamics favors negative tilt on the nightside and positive tilt on the dayside. For example, when the dipole tilt angle is −35° (∼−11.5 diurnal and −23.5 seasonal tilt), GOES will be located in the nightside toward the dusk region (since the rotational axis and the magnetic pole are not perfectly aligned). For a tilt angle of +35°, GOES will be in the dayside dawn region.

The effect of this bias is different in the postmidnight and prenoon. Note that GOES 8, GOES 10, GOES 11, and GOES 12 have different GEO locations, but they are all centered over North America.

3.2. Example of GOES B_y Response to IMF B_y Reversal

Figure 3a shows an example of superposed IMF B_z and B_y components and their standard error of the mean. The *x* axis represents minutes from epoch start. In Figure 3b the mean of the GOES B_y component is shown in blue. The position of GOES is shown in an inset panel in Figure 3b; the position corresponds to the position at $t = 0$. In Figure 3 we have chosen data in the postmidnight sector, from 1 to 4 magnetic local time (MLT) at $t = 0$. This means that the data at $t = -60$ min are from 0 to 3 MLT, while at $t = 180$ the location ranges from 4 to 7 MLT. Therefore, it is not always accurate to compare the different values at different times, since they may correspond to very different regions. The local B_y changes sign at midnight, going from negative in premidnight to positive in postmidnight and eventually reaching a maximum at dawn (or minimum at dusk). The reason for choosing only the spacecraft with locations between 1 and 4 MLT at $t = 0$ min (as shown in Figure 3b) is to avoid inclusion of local times where the local B_y reduction is mainly an orbital effect (B_y, due to the dipole, is negative in the premidnight region and positive in the postmidnight region). The orbit of the spacecraft is the most important factor for the time development of B_y as seen in Figure 3b; however, we can still identify the signatures of the changing IMF B_y: At $t < 0$, IMF B_y is positive and is inducing a positive B_y component in the tail (blue line). The increasing trend seen between $t = -60$ and $t = 0$ in Figure 3b is a combination of the location-dependent strength and the induced field. At $t > 0$ the B_y component is reduced (still increasing but more slowly). The strength of B_y measured by GOES is a combination of an increasing local B_y due to the orbit and an induced negative B_y component. After about 1 h ($t > 60$) the field strength again increases which is due to a combination of the orbit, a weakening IMF B_y, and the fact that for IMF B_y negative the B_y component at dawn (06 MLT) is reduced.

In order to remove the background field, we have used the TS01 combined with International Geomagnetic Reference Field (green line in Figure 3b). The input to TS01 is calculated for each event using OMNI data, but with IMF $B_y = 0$. Setting IMF $B_y = 0$ in the model input is done in order to have a "quiet" background field which we can subtract from the GOES data. Other contributions to the magnetospheric B_y are still included in the TS01 model, which mainly depend on the dipole tilt angle. By setting IMF $B_y = 0$ in TS01, we may underestimate the external magnetic pressure exerted on the magnetosphere ($B_t = \sqrt{B_y^2 + B_z^2}$), which may result in an underestimate of the magnetic field magnitude. However, the effect of the magnetic pressure on the magnetosphere shape and flaring is small compared to the dynamic pressure [see *Petrinec and Russell*, 1996, Table 1]. Even though our baseline may be affected, the magnitude and response and reconfiguration times are still valid.

3.3. Statistical Data Set and Applied Criteria

In this section we describe the criteria applied to the events in order to minimize the effects of other sources of magnetospheric-induced B_y while keeping the events where B_y is induced through dayside reconnection and asymmetric loading of flux. We constructed an algorithm to search for polarity reversals in IMF B_y, either from positive to negative or negative to positive. The algorithm required IMF B_y to be stable, with respect to the polarity, 20 min prior to the reversal and 20 min after. The algorithm further requires IMF ΔB_y to be larger than 2 nT. We found approximately 1600 reversals of each polarity. We further require the SuperMAG SML (similar to the classical *AL* index but derived from more than 300 ground-based magnetometers) index [*Gjerloev*, 2012] to be larger than −200 nT for the nightside events, to avoid strong dipolarization signatures

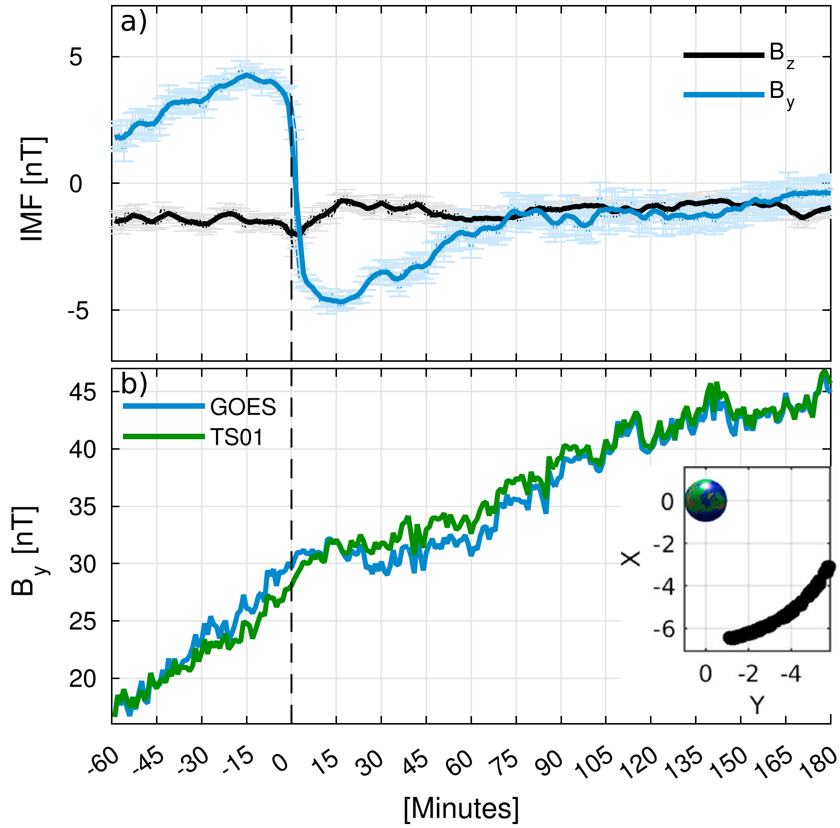

Figure 3. (a) Superposed IMF B_y and B_z components and their standard error of the mean. (b) Superposed B_y component measured by GOES 8, GOES 10, GOES 11, and GOES 12 is shown in blue, and the calculated TS01 B_y component is shown in green. The location shown corresponds to the location at $t = 0$. Around 70 events were used to generate the averages. The *x* axis represents minutes from epoch. All variables are given in SM coordinates.

(related to substorms and magnetotail activity) in the GOES data. We found that substorms add substantial noise to the data. On the dayside this criteria is not as important, and here we set SML > -300. The IMF clock angle $\left(\tan(\theta) = \frac{B_y}{B_z}\right)$ is required to be $290° > \theta > 70°$, favoring dayside reconnection. To avoid bias due to dipole tilt (see section 3.1), we only use data from 23 to 04 MLT region for the nightside. On the dayside we use data between 8.5 and 15.5 MLT.

The uncertainty of the time shift in OMNI is handled by requiring that the standard deviation (given in the OMNI data set) of the time shift is less than 2 min. We note that there is an additional uncertainty in the convection time from the bow shock nose to the magnetopause subsolar point. Throughout the paper we use the presumed arrival of the IMF phase front reversals at the bow shock as our reference point. Finally, we also require the average dipole tilt angle to be close to zero ($<10°$) such that any effect of this source averages out. The effects of tilt will be discussed in section 5.

4. Determining Response and Reconfiguration Times From Observations

In this section we show how the nightside and dayside magnetosphere respond to an abrupt IMF B_y reversal. We present two different IMF transitions of IMF B_y: a reversal from negative to positive (Figure 4) and positive to negative (Figure 5).

Figures 4a, 4a′, 5a, and 5a′ show the IMF conditions where the error bars represent the standard error of the mean. Figures 4b, 4b′, 5b, and 5b′ show both the mean and median of the field measured by GOES with the background TS01 B_y subtracted. Error bars represent standard error of the mean. The bar plots in the second panels (b,b′) show the number of events.

4.1. GOES B_y Response to Negative to Positive IMF B_y Transitions

Figure 4 shows the superposed epoch B_y response at GOES for the dayside and nightside, respectively.

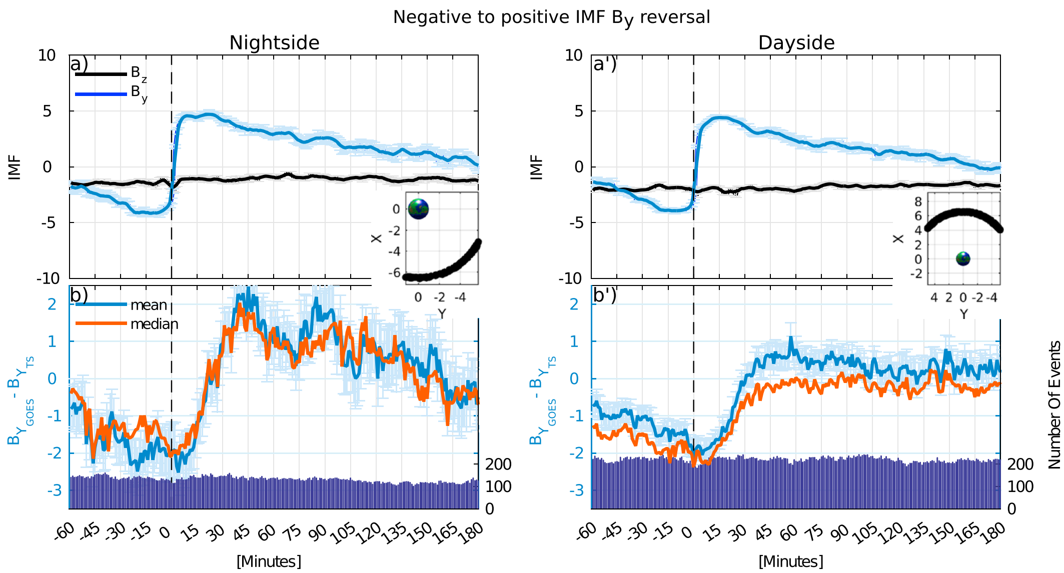

Figure 4. (a and a′) Averaged IMF B_y and B_z with error bars corresponding to standard error of the mean. (b and b′) The mean (blue) and median (red) B_y component measured by GOES with the TS01 field subtracted. Bar plot in Figures 4b and 4b′ shows number of events, about 100 for nightside and 200 for dayside. The x axis represents minutes from epoch. The embedded figures show the location of GOES at $t = 0$.

For both the dayside (Figures 4a′ and 4b′) and the nightside IMF B_y reverses from approximately −4 nT to +4 nT. The solar wind velocity was on average 450 km/s and 455 km/s for the nightside and dayside, respectively. About 30 min after the reversal, IMF B_y weakens and the standard error of the mean increases. Due to the motion of the GOES spacecraft, caution must be taken when interpreting the IMF and magnetospheric signatures for anything but the large-scale trends after $t = 30$ min. Figures 4b and 4b′ show the GOES B_y component response to the IMF B_y reversal. There is no significant difference between the mean and the median, suggesting that the mean is robust. As seen in Figures 4b and 4b′, there is a pronounced difference between the response at the nightside and dayside: the induced B_y is larger on the nightside. Also, the slope of GOES B_y is steeper on the nightside. The mean and median values on the nightside are calculated from about 100 events, whereas the dayside results are based on around 200 events. It is evident that the baseline

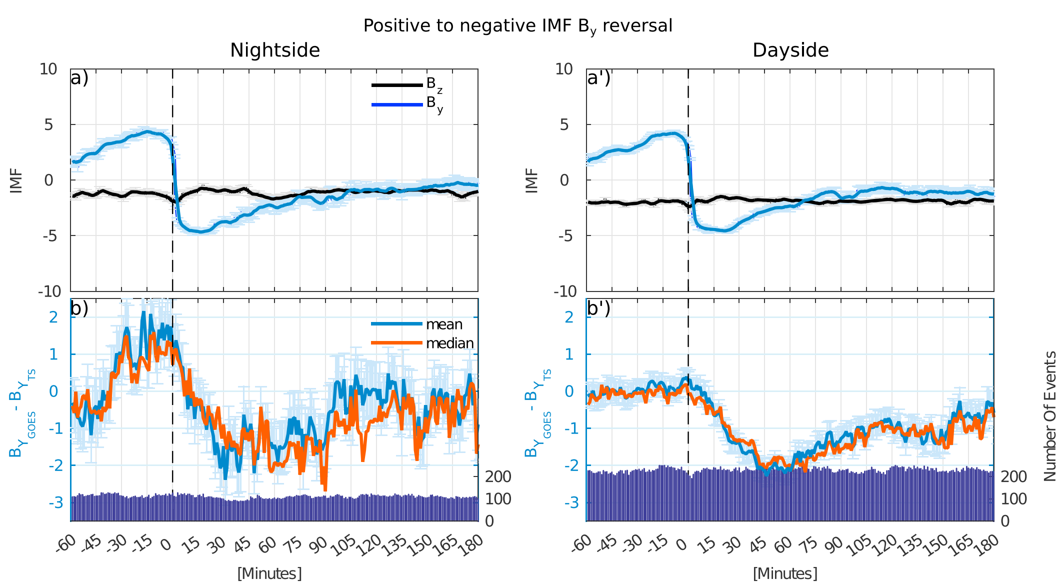

Figure 5. As in Figure 3 but now for the opposite IMF reversal.

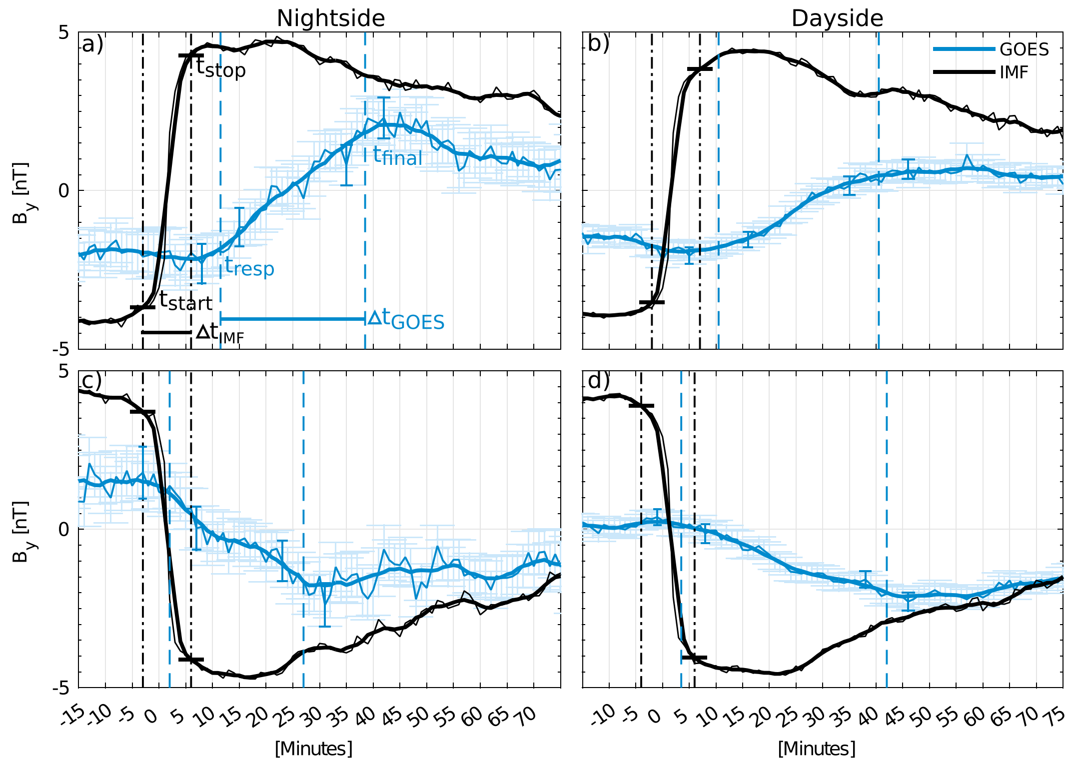

Figure 6. IMF B_y (black) and GOES B_y correspond to (a, b) Figure 4 and (c, d) Figure 5 but are smoothed using a moving average with 10 min step length. The black vertical dash-dotted lines show the defined t_{start}, the time when IMF B_y begins to the reverse, and t_{stop} indicates the time when IMF B_y ends its rotation. The blue vertical dashed lines show the defined GOES response and the GOES final time. The uncertainty in GOES B_y represents the standard error of the mean. See text for details and Table 1 for values.

is not correctly determined by the TS01 model on the dayside, as the mean and median are both close to zero for positive IMF B_y ($t < 0$ min). This is also the case for the opposite reversal seen in Figure 5b′.

4.2. Positive to Negative IMF B_y Transitions

Figure 5 shows the response to an IMF B_y reversal from positive to negative for the same locations, under similar conditions and similar number of events as in Figure 4. For both the dayside and the nightside IMF B_y reverses from approximately +4 nT to −4 nT. The solar wind velocity is on average 441 and 443 km/s for the nightside and dayside, respectively. Similar to Figure 4, the magnitude of the induced B_y in Figure 5 is larger on the nightside. Also, the baseline of Figure 5b′ is not correctly determined in this state either (see Figure 4b′). However, the response and the reconfiguration times should not be affected.

On the nightside, for both IMF B_y reversals, the magnitudes of the induced B_y component are comparable. The "induction efficiency" describes the ratio between the strength of the IMF ΔB_y nT to the GOES ΔB_y. For the nightside GOES $\Delta B_y \sim 4$, while IMF $\Delta B_y \sim 8$ nT. The resulting efficiency is about 53% (induced $B_y = 0.53 \cdot$ IMF B_y) in Figure 4a and ∼48% in Figure 5a. On the dayside $\Delta B \sim 2.5$ nT, resulting in an induction efficiency of ∼30% for both IMF B_y transitions. Note that these are average values for all solar wind speeds.

4.3. Characteristic Response and Reconfiguration Times

To determine the time between IMF B_y reversals (t_{start}) and the corresponding B_y response at GOES (t_{resp}), we have filtered the data using a running mean with a 10 min step length (see Figure 6). The 10 min interval was chosen as the lowest interval that gives a smooth curve (for the nightside) that could be used to define the lower bounds. By visual inspection, we identify the first signature of changes in B_y. This is defined as our lower bound. The upper bound is determined by the standard error of the mean, by identifying the first value outside the uncertainty of our lower bound as illustrated in Figure 6a. The same method has been applied to determine t_{final} and IMF t_{stop}. We emphasize that we are not using the smoothed running mean to determine the response time directly; instead, it is used to determine the lower bound. Table 1 summarizes the observed response and reconfiguration time and their uncertainties. Note that approximately 5 min should

Table 1. IMF B_y and GOES B_y Response and Reconfiguration Times; See Figure 6[a]

	IMF				GOES			Ratio
	Epoch Start t_e(min)	Start t_{start}	Stop t_{stop}	Δt_{IMF}	Response t_{resp}	Final t_{final}	Δt_{GOES}	$\Delta t_{GOES}/\Delta t_{IMF}$
Nightside $\pm B_y$	-3 ± 2	0 ± 2	9 ± 2	9 ± 2.8	14.5 ± 3.5	41.5 ± 3.5	27 ± 5	3.0 ± 0.35
Dayside $\pm B_y$	-2 ± 2	0 ± 2	9 ± 2	9 ± 2.8	12.5 ± 5.5	42.5 ± 5.5	30 ± 8	3.3 ± 0.4
Nightside $\pm B_y$	-3 ± 2	0 ± 2	9 ± 2	9 ± 2.8	5 ± 5	30 ± 4	25 ± 6.4	2.8 ± 0.4
Dayside $\pm B_y$	-4 ± 2	0 ± 2	10 ± 2	10 ± 2.8	7.5 ± 4.5	46 ± 4	38.5 ± 6	3.85 ± 0.32

[a]All times are relative to the bow shock reference time. Note that there is an additional 4–8 min for the IMF phase fronts to propagate from the bow shock to the upstream magnetopause.

be subtracted from the GOES response and reconfiguration time to account for the propagation from the bow shock to the subsolar point. The response and reconfiguration times from the presumed arrival at the magnetopause are presented in parentheses in the following section.

From Table 1 we conclude that the magnetospheric response time, at all local time positions, is less than 15 ($\sim$10) min from the bow shock (magnetopause) arrival time. In less than 46 ($\sim$41) min the magnetospheric state has reached its final configuration (t_{final}). Δt_{IMF} and Δt_{GOES} are defined as the times between the beginning and end of the reversals. The ratio $\Delta t_{GOES}/\Delta t_{IMF}$ describes the relationship between the slope of IMF B_y and the magnetospheric B_y; thus, it describes how quickly the magnetosphere reconfigures with respect to the time it takes IMF B_y to rotate. From Table 1 we can see that the reconfiguration in the magnetosphere takes about 3 times longer than the duration of the IMF reversals.

For both types of reversals on the dayside and nightside, the magnetic field topology changes from a positive (or negative) B_y state to a configuration where the induced B_y has vanished after about 25 ($\sim$20) min. This means that the tilted field lines have rectified or straightened out. This is determined simply by identifying the time halfway from peak to peak. For events where the IMF B_y changes rapidly from zero to some value, one should expect to observe a significant induced B_y component during this time scale. In terms of response and reconfiguration times, Figures 6a, 6b, and 6d reveal similar behavior. IMF B_y positive to negative transitions (at least on the nightside—see Figure 6c) show a faster response. This observation is interesting and intriguing, and we do not have good explanation for it.

4.4. What Controls the Response and Reconfiguration Time?

The coupling efficiency between the solar wind and the magnetosphere is often described by empirical relations, e.g., the Akasofu ϵ parameter [*Perreault and Akasofu*, 1978] or more refined versions [*Milan et al.*, 2012; *Tenfjord and Østgaard*, 2013].

These coupling functions usually contain the solar wind speed, clock angle, density, and the magnetic field. One could argue that a coupling function describing the transport of magnetic flux across the magnetopause would be correlated with the reconfiguration time, as a higher rate of asymmetric loading of flux in the lobes should result in stronger pressure gradients. To check whether the amplitude of the IMF B_y reversals or the solar wind velocity results in a different reconfiguration or efficiency, we grouped the data according to these parameters. To determine the role of the IMF B_y magnitude, we sorted the events in IMF ΔB_y magnitude. In Figure 7, we selected only events where IMF $B_y < -3$ nT prior to the reversal and IMF $B_y > 3$ nT after the reversal. Thus, the average value of $\Delta B_y = 14$ nT means that the IMF reversal is from -7 nT to $+7$ nT. Figure 7 shows both the nightside (a) and the dayside (b) separately. The impact is clearer on the nightside (Figure 7a). The first pair, yellow and purple, shows the response for different IMF ΔB_y values for events with high solar wind velocity. Values together with number of events are given in the legend of Figure 7. For the purple line on the nightside (Figure 7a), the "high solar wind" velocity constraint is $V > 350$ km/s versus $V > 400$ km/s for the dayside (Figure 7b), due to few events in this group. The second pair, green and black, shows the response for slow solar wind velocity $V < 450$ km/s and two different IMF ΔB_y values. On the nightside (Figure 7a) it is evident that higher solar wind velocity results in a quicker reconfiguration time and a larger magnitude of the induced B_y (compare yellow and green lines). Comparing yellow with purple, the magnitude of GOES ΔB_y is comparable; however, since the IMF ΔB_y is larger, the induction efficiency is lower. Comparing purple and black (large IMF ΔB_y, slow and fast solar wind velocity), the purple line has a larger GOES ΔB_y and slightly

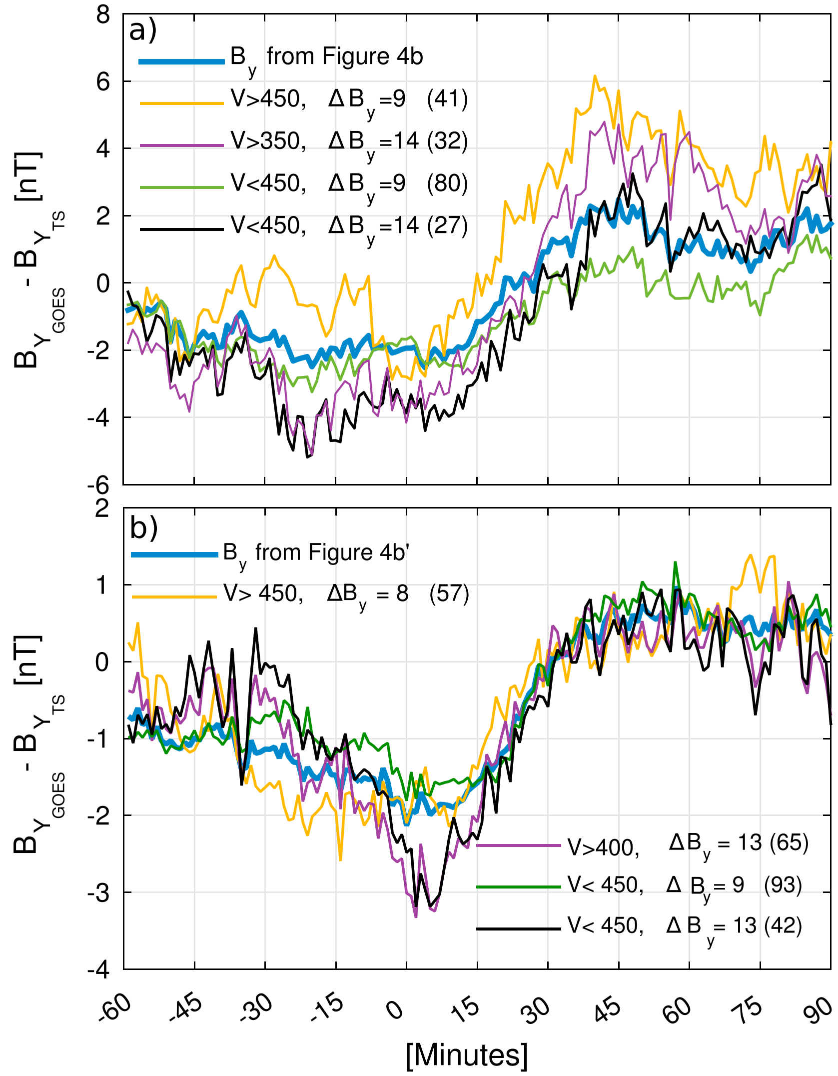

Figure 7. Mean value of GOES B_y-TS01 B_y for different solar wind velocities and IMF reversal strength on the (a) nightside and (b) dayside. In the legends, V corresponds to the absolute value of the solar wind velocity and ΔB represents the magnitude of the change of the IMF B_y reversal. Blue lines (in Figures 7a and 7b) are the same as in Figures 4b and 4b'. See text for details.

quicker reconfiguration, again suggesting that the velocity has a larger influence on the induction efficiency and reconfiguration time. For the dayside (Figure 7b) the difference (purple and black) in the reconfiguration time is not apparent. It shows that a larger IMF ΔB_y results in a larger GOES ΔB_y; however, the induction efficiency remains the same.

Higher solar wind velocities lead to faster loading of asymmetric magnetic flux from the dayside reconnection site to the lobes, which results in quicker reconfiguration, and larger magnitude (thus also efficiency) of the induced B_y. Stronger IMF B_y results in a larger asymmetric pressure buildup in the magnetosphere and therefore in a larger induced B_y [see *Tenfjord et al.*, 2015]. The efficiency for the events with $V_{SW} > 450$ km/s on the nightside (yellow line) is close to 90%, while for the purple line it is about 58%, which means that higher velocity results in higher efficiency. From Figure 7a we conclude that at the nightside the reconfiguration time is quicker, and the magnitude (ΔB_y) is larger for higher solar wind velocity and stronger IMF B_y. It is not clear on either of the regions if the solar wind velocity or the magnitude of IMF B_y influences the response time.

A similar trend, albeit not as clear, is seen when sorting the data according to the solar wind dynamic plasma pressure, suggesting that the velocity is dominating over the density.

5. Discussion

The objective of this study has been to determine how fast the B_y component on closed field lines is induced and how the magnetic field reconfigures in response to changes in the IMF B_y component. We have suppressed effects of other B_y inducing mechanisms by setting constraints on the data, such as clock angle, dipole tilt angle, and SML index. Now we will discuss consequences of our findings and how these compare to earlier work.

5.1. Timing

We have shown that magnetic field at geosynchronous orbit responds to an IMF B_y transition within 15 (10) min from the presumed arrival at the bow shock (magnetopause). No significant differences in response and reconfiguration times between the dayside and nightside are apparent in the timing analysis. On average there is a difference between the response of negative to positive (Figure 4) and positive to negative (Figure 5). For both regions, a positive to negative transition results in a faster response time compared to the opposite transition. Presently, we have no explanation for this behavior.

Tenfjord et al. [2015] used MHD simulations to show that the pressure distribution inside the magnetosphere becomes asymmetric after about 10 min. This asymmetric pressure excites plasma flows which in turn induce a B_y component on the surrounding closed field lines. The response times presented here correspond to the buildup of this region of enhanced magnetic pressure and the propagation of the compressional Alfvén wave from the lobes to the inner magnetosphere.

Tenfjord et al. [2015] modeled the response of the IMF B_y changing from zero to 10 nT as a simple step function. The authors showed that after 25 min, a magnetospheric B_y component was established at $L = 11\ R_E$ on the nightside. Although t_{resp} and t_{final} differ between the nightside, dayside and polarities, the ratio $\frac{\Delta t_{\mathrm{GOES}}}{\Delta t_{\mathrm{IMF}}}$ is remarkably stable. From Table 1 the ratio between Δt_{GOES} and Δt_{IMF} has an average value of about 3.2. The ratio indicates that for their step function IMF B_y transition the final reconfiguration time should be close to 30 min. For this reason the conclusion in *Tenfjord et al.* [2015] that the IMF B_y induces a B_y component on closed field lines on times scales of tens of minutes is in agreement with the empirical results of this study. *Tenfjord et al.* [2015] found a shorter reconfiguration time on the dayside. The results from this paper indicate that this is not the case.

In Figure 7 we saw that the reconfiguration time depends mainly on the solar wind velocity and to a lesser extent on the magnitude of IMF B_y. Higher solar wind velocity results in faster loading of asymmetric flux which means a quicker reconfiguration and larger induced B_y.

Motoba et al. [2011] reported a case study with 51 min time delay between the IMF clock angle change and the Cluster B_y component. The authors performed a cross correlation between the IMF clock angle and the four Cluster spacecraft located near midnight between 12 and 14 R_E. In the period of their cross correlation, two substorms occurred and magnetotail activity was high. We interpret the prominent magnetic field signatures in *Motoba et al.* [2011] as a signature of bursty bulk flows [*Birn et al.*, 2011] launched along the Sun-Earth line (duskward of Cluster). This interpretation is strengthened by the fact that it is observed first by Cluster 2, which is closest to midnight, and last by Cluster 1, which is farthest from midnight (toward dawn). The localized dip in magnetotail B_y seen in *Motoba et al.*'s [2011] Figure 2 after it has started to increase can be interpreted as signatures of a plasma-depleted flux tube [*Sergeev et al.*, 1996] as it coincides with a significant decrease in the plasma pressure. Thus, it is possible that the observed B_y change reflects internal configuration within the magnetosphere during bursty bulk flows, instead of a direct consequence of IMF B_y. Also, *Motoba et al.*'s [2011] prominent feature is a reversal in IMF B_y from negative to positive, followed by a positive to negative reversal [*Motoba et al.*, 2011, Figure 2]. The IMF B_y is positive for only 15 min. As we have shown, at geostationary distances, it takes the magnetospheric field 3 times longer to completely reconfigure (Table 1). Therefore, we expect the magnitude of the induced B_y component to be weak (low induction efficiency), yet the efficiency in the event *Motoba et al.* [2011] analyzed is more than 100%. *Motoba et al.* [2011] determined the time lag by cross correlation. As our results show, the magnetosphere and ionosphere can respond almost immediately to changes in solar wind but reconfigure more slowly. Therefore, cross correlation will not always give the correct time lags, as it will relate to the most prominent signals between the two data sets, such as the peaks of magnetic perturbations [*Lu et al.*, 2002]. Also, due to the relatively long reconfiguration time, there is not a linear correlation between the IMF B_y and the magnetospheric B_y, and a high correlation coefficient should not be expected.

Rong et al. [2015] reported 1–1.5 h lag time between the IMF B_y and magnetotail B_y, based on two events. Both events are chosen to coincide with a strong solar wind dynamic pressure pulse, and in both cases the IMF B_z is northward. We believe that during postive IMF B_z and nonzero IMF B_y, dayside lobe reconnection will transport lobe flux from dusk to dawn (or dawn to dusk depending on the polarity of IMF B_y) and set up pressure gradients which will affect the closed magnetosphere (as for IMF $B_z < 0$ and IMF B_y). However, we do not know how efficient this will be and what the associated time scales would be. In the events studied by *Rong et al.* [2015] there is a pressure pulse coinciding with the IMF B_y change which may mask earlier signatures of any change in IMF-induced B_y. Analyzing such events and separating spatiotemporal changes from IMF-induced effects is problematic. For instance, in the second event analyzed by *Rong et al.* [2015], the identified response time in the magnetotail coincides with the time B_x changes sign. Thus, it is expected that B_y also will change, in the manner seen in their figure. For these reasons, we do not agree with the interpretation given by *Rong et al.* [2015].

5.2. Coupling Efficiency

In this section we compare the efficiency of IMF B_y in generating a B_y component on closed field lines to earlier work. In contrast to many of the other studies, we have used the TS01 model as our background field. Even though we have IMF $B_y = 0$ in the model input, the TS01 model has incorporated other processes for generating B_y which may influence the efficiency when compared to earlier results. Our results from the dayside magnetosphere indicate a change in B_y strength of ~2.5 nT at geosynchronous orbit in response to $\Delta B \sim 8$ nT IMF B_y change. The B_y coupling efficiency is about 30%. For the nightside, we find 48–53% efficiency. For comparison, *Petrukovich* [2009] found that the penetration efficiency increases from approximately 35% at $X = -30$ to 65% at $X = -12\,R_E$. *Wing et al.* [1995] found an efficiency of 29% at noon and 79% around midnight at geosynchronous locations. The authors note that by binning the data such that it covers 6 h in local time, centered around midnight, the efficiency drops to 36% on the nightside. *Cowley and Hughes* [1983] found $37 \pm 8\%$ for the nightside and $23 \pm 5\%$ at noon, during southward IMF B_z, in agreement with our result. *Cowley and Hughes* [1983] also noted that the highest correlation was found for zero time delay between the solar wind data and geostationary B_y, suggesting that the response is less than their 1 h resolution. *Stenbaek-Nielsen and Otto* [1997] suggested that the strength of the magnetospheric B_y component depends on radial distances. *Lui* [1984] found the efficiency to be 50% between $-30\,R_E < X < -10\,R_E$, while *Fairfield* [1979] found 13% between $-30\,R_E < X < -10\,R_E$ (entire magnetotail). Further earthward, *Wing et al.* [1995] found 79% (or 36% as discussed above) at midnight. We argue that the pressure distribution in the lobes due to asymmetric loading of newly reconnected flux from the dayside reconnection determines the magnitude and the distribution of the induced B_y component. This was discussed in section 3.2 in *Tenfjord et al.* [2015] and shown in their Figure 2.

Stenbaek-Nielsen and Otto [1997] suggested that since B_y is induced nonuniformly in the magnetotail, there should exist a region where the efficiency is maximum and a minimum region close to Earth where the dipole field dominates. The authors considered B_y on closed field lines to arise due to tail reconnection of field lines with asymmetric foot points. Due to the pileup effect [*Hau and Erickson*, 1995], they suggested that the region of maximum B_y would exist somewhere between the reconnection site and Earth. Even though the results presented here do not indicate a region of maximum efficiency, we have now shown that an induced B_y arises on closed field lines independently of tail reconnection. Thus, the quickly induced B_y is a strong indication that asymmetric magnetic pressure loaded through dayside reconnection controls the distribution of B_y in the magnetotail.

The induction efficiency is lower on the dayside for both IMF B_y reversals. As explained above, the loading of asymmetric flux creates a region of enhanced pressure in the two lobes. This region excites plasma flows (v_y) via the momentum equation: $\rho \frac{\mathrm{d}v_y}{\mathrm{d}t} = \frac{-1}{2\mu_0} \frac{\partial}{\partial y}(B_x^2 + B_z^2)$ [*Tenfjord et al.*, 2015, equation 2]. We suggest that since the dayside magnetic field is more compressed compared to the nightside, the asymmetric loading of magnetic flux will result in a weaker gradient on the dayside. The shear flows (which in turn induces the B_y component) will be weaker on the dayside of the dawn-dusk meridian compared to the nightside. This argument is equivalent to stating that the stiffness of the inner magnetospheric field is greater on the dayside compared to the nightside on geosynchronous distances.

5.3. Mechanisms Responsible for Inducing B_y in the Magnetotail

Internal processes may also influence the induction efficiency. We found the dipole tilt angle to be a significant source of magnetospheric B_y. We noted in section 1 that a tilt bias exists in the GOES data, favoring negative tilt on the nightside dusk region. The warped current sheet arising as a consequence of the dipole tilt [*Tsyganenko and Fairfield*, 2004] will affect the resulting B_y component [e.g., *Liou and Newell*, 2010, Figure 3]. While we see significant contributions from the dipole tilt angle effect, we were unable to quantify a systematic behavior depending on IMF B_y polarity, tilt, and region in our limited data set.

We also saw dawn-dusk asymmetries in the magnitude of magnetospheric ΔB. Some of these asymmetries appear to be related to dipole tilt effects. Some of these effects become mitigated by the subtraction of TS01 as the background field, so that whatever remains could be unsystematic residuals (see discussion in *Petrukovich* [2009]). Using Geotail data, *Petrukovich* [2009] found the tilt effect to be uneven in both radial distance and in the postmidnight and premidnight regions. They identified regions in the magnetotail where the average addition to B_y due to the tilt effects was maximum and minimum (see their Figure 7). For instance, it was found that in the region $X > -20\,R_E$ and $0 < Y < 10\,R_E$ the effect is 4 times stronger compared to neighboring regions. Due to the orbit of Geotail, *Petrukovich* [2009] only analyzed $X < -8\,R_E$. We observe similar asymmetries at geosynchronous orbit, consistent with their results. Analyzing these asymmetries is outside the scope of this paper.

As mentioned, we set constraints on the data in order to keep the dipole tilt angle comparable between the different polarities. We required the dipole tilt angle to be on average close to zero ($|\mathrm{tilt}| < 10°$). Nevertheless, there are differences in the dipole tilt angle during the time intervals. On the dayside, the dipole tilt is positive $\sim$8° at $t = 0$ and declining to about 2° at $t = 240$ min, for both states. On the nightside, for both polarities, the dipole tilt angle is negative, starting at about $\sim$−8° at $t = 0$ and increasing to 0 at $t = 240$ min. Additionally, even though the evolution of the dipole tilt is comparable for each region, there are differences. According to *Liou and Newell* [2010] (see their Figure 3), a negative tilt angle favors a positive B_y in the postmidnight region. Thus, we should expect Figure 4b to show a stronger induced B_y compared to Figure 5b. No such signature is seen. On the dayside the effect would be opposite; however, since the locations of the spacecraft are more evenly distributed between the prenoon and postnoon regions, it is not likely that this is contributing to the differences between the response.

Other mechanisms able to generate a B_y component on closed magnetospheric field lines discussed in section 1 are considered small or negligible in the region we have studied.

6. Summary

The results of this paper can be summarized as follows:

1. The magnetosphere responds to a change in IMF B_y in less than 15 ($\sim$10) min in all local time sectors from the presumed arrival at the bow shock (magnetopause).
2. At geosynchronous distances, the reconfiguration time is less than 45 ($\sim$40) min in all local time sectors.
3. The response time is consistent with asymmetric loading of flux to the lobes.
4. A B_y component is induced on closed field lines independently of tail reconnection.
5. On the nightside, the reconfiguration time and the magnitude of the induced B_y component depend on the solar wind velocity.
6. The positive-to-negative and the negative-to-positive B_y transitions have significantly different response characteristics, but the ratio $\Delta t_{\mathrm{GOES}}/\Delta t_{\mathrm{IMF}}$ is remarkably similar.

Acknowledgments
This study was supported by the Research Council of Norway/CoE under contract 223252/F50. S.E. Milan was supported by STFC grant ST/K001000/1. We acknowledge the use of NASA/GSFC's Space Physics Data Facility for OMNI data. For the ground magnetometer data we gratefully acknowledge the following: Intermagnet; USGS, Jeffrey J. Love; CARISMA, PI Ian Mann; CANMOS; the S-RAMP Database, PI K. Yumoto and K. Shiokawa; the SPIDR database; AARI, PI Oleg Troshichev; the MACCS program, PI M. Engebretson, Geomagnetism Unit of the Geological Survey of Canada; GIMA; MEASURE, UCLA IGPP, and Florida Institute of Technology; SAMBA, PI Eftyhia Zesta; 210 Chain, PI K. Yumoto; SAMNET, PI Farideh Honary; the institutes who maintain the IMAGE magnetometer array, PI Eija Tanskanen; PENGUIN; AUTUMN, PI Martin Connors; DTU Space, PI Juergen Matzka; South Pole and McMurdo Magnetometer, PIs Louis J. Lanzarotti and Alan T. Weatherwax; ICESTAR; RAPIDMAG; PENGUIN; British Antarctic Survey; McMac, PI Peter Chi; BGS, PI Susan Macmillan; Pushkov Institute of Terrestrial Magnetism, Ionosphere and Radio Wave Propagation (IZMIRAN); GFZ, PI Juergen Matzka; MFGI, PI B. Heilig; IGFPAS, PI J. Reda; University of L'Aquila, PI M. Vellante; and SuperMAG, PI Jesper W. Gjerloev. The OMNI and GOES data are found here: http://cdaweb.gsfc.nasa.gov. SuperMAG data are available here: http://supermag.jhuapl.edu/. Scientists interested in other data used should contact the corresponding author.

References

Angelopoulos, V., W. Baumjohann, C. F. Kennel, F. V. Coroniti, M. G. Kivelson, R. Pellat, R. J. Walker, H. Lühr, and G. Paschmann (1992), Bursty bulk flows in the inner central plasma sheet, *J. Geophys. Res.*, *97*(A4), 4027–4039, doi:10.1029/91JA02701.

Birn, J., R. Nakamura, E. V. Panov, and M. Hesse (2011), Bursty bulk flows and dipolarization in MHD simulations of magnetotail reconnection, *J. Geophys. Res.*, *116*, A01210, doi:10.1029/2010JA016083.

Caan, M., R. McPherron, and C. Russell (1975), Substorm and interplanetary magnetic field effects on the geomagnetic tail lobes, *J. Geophys. Res.*, *80*(1), 191–194, doi:10.1029/JA080i001p00191.

Cao, J., A. Duan, M. Dunlop, W. Xinhua, and C. Cai (2014), Dependence of IMF B_y penetration into the neutral sheet on IMF Bz and geomagnetic activity, *J. Geophys. Res. Space Physics*, *119*, 5279–5285, doi:10.1002/2014JA019827.

Cowley, S. (1981), Magnetospheric asymmetries associated with the y-component of the IMF, *Planet. Space Sci.*, *29*(1), 79–96, doi:10.1016/0032-0633(81)90141-0.

Cowley, S., and W. Hughes (1983), Observation of an IMF sector effect in the Y magnetic field component at geostationary orbit, *Planet. Space Sci.*, *31*(1), 73–90, doi:10.1016/0032-0633(83)90032-6.

Dudeney, J. R., A. S. Rodger, M. P. Freeman, J. Pickett, J. Scudder, G. Sofko, and M. Lester (1998), The nightside ionospheric response to IMF By changes, *Geophys. Res. Lett.*, *25*(14), 2601–2604, doi:10.1029/98GL01413.

Fairfield, D. H. (1979), On the average configuration of the geomagnetic tail, *J. Geophys. Res.*, *84*, 1950–1958, doi:10.1029/JA084iA05p01950.

Fear, R. C., and S. E. Milan (2012), The IMF dependence of the local time of transpolar arcs: Implications for formation mechanism, *J. Geophys. Res.*, *117*, A03213, doi:10.1029/2011JA017209.
Friis-Christensen, E., Y. Kamide, A. D. Richmond, and S. Matsushita (1985), Interplanetary magnetic field control of high-latitude electric fields and currents determined from Greenland Magnetometer Data, *J. Geophys. Res.*, *90*(A2), 1325–1338, doi:10.1029/JA090iA02p01325.
Gjerloev, J. W. (2012), The SuperMAG data processing technique, *J. Geophys. Res.*, *117*, A09213, doi:10.1029/2012JA017683.
Grocott, A., and S. E. Milan (2014), The influence of IMF clock angle timescales on the morphology of ionospheric convection, *J. Geophys. Res. Space Physics*, *119*, 5861–5876, doi:10.1002/2014JA020136.
Haaland, S., G. Paschmann, and B. U. . Sonnerup (2006), Comment on "A new interpretation of Weimer et al.'s solar wind propagation delay technique" by Bargatze et al., *J. Geophys. Res.*, *111*, A06102, doi:10.1029/2005JA011376.
Hau, L., and G. Erickson (1995), Penetration of the interplanetary magnetic field B_y into Earth's plasma sheet, *J. Geophys. Res.*, *100*(2), 745–751.
Jackel, B. J., B. McKiernan, and H. J. Singer (2012), Geostationary magnetic field response to solar wind pressure variations: Time delay and local time variation, *J. Geophys. Res.*, *117*, A05203, doi:10.1029/2011JA017210.
Kabin, K., R. Rankin, R. Marchand, T. I. Gombosi, C. R. Clauer, A. J. Ridley, V. O. Papitashvili, and D. L. DeZeeuw (2003), Dynamic response of Earth's magnetosphere to B_y reversals, *J. Geophys. Res.*, *108*, 1–13, doi:10.1029/2002JA009480.
Khan, H., and S. Cowley (1999), Observations of the response time of high-latitude ionospheric convection to variations in the interplanetary magnetic field using EISCAT and IMP-8 data, *Ann. Geophys.*, *17*(10), 1306–1335, doi:10.5194/angeo-17-1306-1999.
Khurana, K. K., R. J. Walker, and T. Ogino (1996), Magnetospheric convection in the presence of interplanetary magnetic field B_y: A conceptual model and simulations, *J. Geophys. Res.*, *101*, 4907–4916.
King, J. H., and N. E. Papitashvili (2005), Solar wind spatial scales in and comparisons of hourly Wind and ACE plasma and magnetic field data, *J. Geophys. Res.*, *110*, A02104, doi:10.1029/2004JA010649.
Kullen, A., and P. Janhunen (2004), Relation of polar auroral arcs to magnetotail twisting and IMF rotation: A systematic MHD simulation study, *Ann. Geophys.*, *22*(3), 951–970, doi:10.5194/angeo-22-951-2004.
Liou, K., and P. T. Newell (2010), On the azimuthal location of auroral breakup: Hemispheric asymmetry, *Geophys. Res. Lett.*, *37*, L23103, doi:10.1029/2010GL045537.
Lu, G., T. E. Holzer, D. Lummerzheim, J. M. Ruohoniemi, P. Stauning, O. Troshichev, P. T. Newell, M. Brittnacher, and G. Parks (2002), Ionospheric response to the interplanetary magnetic field southward turning: Fast onset and slow reconfiguration, *J. Geophys. Res.*, *107*, 1–9, doi:10.1029/2001JA000324.
Lui, A. T. Y. (1984), Characteristics of the cross-tail current in the Earth's magnetotail, in *Magnetospheric Currents*, edited by T. A. Potemra, pp. 158–170, AGU, Washington, D. C., doi:10.1029/GM028p0158.
Lyon, J. G., J. A. Fedder, and C. M. Mobarry (2004), The Lyon-Fedder-Mobarry (LFM) global MHD magnetospheric simulation code, *J. Atmos. Sol. Terr. Phys.*, *66*, 1333–1350, doi:10.1016/j.jastp.2004.03.020.
Merkin, V. G., B. J. Anderson, J. G. Lyon, H. Korth, M. Wiltberger, and T. Motoba (2013), Global evolution of Birkeland currents on 10 min timescales: MHD simulations and observations, *J. Geophys. Res. Space Physics*, *118*, 4977–4997, doi:10.1002/jgra.50466.
Milan, S. E., J. S. Gosling, and B. Hubert (2012), Relationship between interplanetary parameters and the magnetopause reconnection rate quantified from observations of the expanding polar cap, *J. Geophys. Res.*, *117*, 1–16, doi:10.1029/2011JA017082.
Motoba, T., K. Hosokawa, Y. Ogawa, N. Sato, A. Kadokura, S. C. Buchert, and H. Réme (2011), In situ evidence for interplanetary magnetic field induced tail twisting associated with relative displacement of conjugate auroral features, *J. Geophys. Res.*, *116*(4), 1–7, doi:10.1029/2010JA016206.
Nishida, A. (1968), Coherence of geomagnetic DP 2 fluctuations with interplanetary magnetic variations, *J. Geophys. Res.*, *73*, 5549–5559, doi:10.1029/JA073i017p05549.
Østgaard, N., S. B. Mende, H. U. Frey, T. J. Immel, L. A. Frank, J. B. Sigwarth, and T. J. Stubbs (2004), Interplanetary magnetic field control of the location of substorm onset and auroral features in the conjugate hemispheres, *J. Geophys. Res.*, *109*, A07204, doi:10.1029/2003JA010370.
Østgaard, N., K. M. Laundal, L. Juusola, A. Åsnes, S. E. Haaland, and J. M. Weygand (2011), Interhemispherical asymmetry of substorm onset locations and the interplanetary magnetic field, *Geophys. Res. Lett.*, *38*, L08104, doi:10.1029/2011GL046767.
Parker, E. N. (1996), The alternative paradigm for magnetospheric physics, *J. Geophys. Res.*, *101*, 10,587–10,625, doi:10.1029/95JA02866.
Parker, E. N. (2007), *Conversations on Electric and Magnetic Fields in the Cosmos*, Princeton Univ. Press Princeton, N. J.
Perreault, P., and S. I. Akasofu (1978), A study of geomagnetic storms, *Geophys. J. R. Astron. Soc.*, *54*(3), 547–573, doi:10.1111/j.1365-246x.1978.tb05494.x.
Petrinec, S. M., and C. T. Russell (1996), Near-Earth magnetotail shape and size as determined from the magnetopause flaring angle, *J. Geophys. Res.*, *101*, 137–152, doi:10.1029/95JA02834.
Petrukovich, A. A. (2009), Dipole tilt effects in plasma sheet B_y: Statistical model and extreme values, *Ann. Geophys.*, *27*(3), 1343–1352, doi:10.5194/angeo-27-1343-2009.
Petrukovich, A. A. (2011), Origins of plasma sheet B_y, *J. Geophys. Res.*, *116*, A07217, doi:10.1029/2010JA016386.
Ridley, A. J., and C. R. Clauer (1996), Characterization of the dynamic variations of the dayside high-latitude ionospheric convection reversal boundary and relationship to interplanetary magnetic field orientation, *J. Geophys. Res.*, *101*, 10,919–10,938, doi:10.1029/JA101iA05p10919.
Rong, Z. J., A. T. Y. Lui, W. X. Wan, Y. Y. Yang, C. Shen, A. A. Petrukovich, Y. C. Zhang, T. L. Zhang, and Y. Wei (2015), Time delay of interplanetary magnetic field penetration into Earth's magnetotail, *J. Geophys. Res. Space Physics*, *120*, 3406–3414, doi:10.1002/2014JA020452.
Ruohoniemi, J. M., S. Shepherd, and R. Greenwald (2002), The response of the high-latitude ionosphere to IMF variations, *J. Atmos. Sol. Terr. Phys.*, *64*, 159–171, doi:10.1016/S1364-6826(01)00081-5.
Sergeev, V. A., V. Angelopoulos, J. T. Gosling, C. A. Cattell, and C. T. Russell (1996), Detection of localized, plasma-depleted flux tubes or bubbles in the midtail plasma sheet, *J. Geophys. Res.*, *101*(A5), 10,817–10,826, doi:10.1029/96JA00460.
Singer, H. J., L. Matheson, R. Grubb, A. Newman, and S. D. Bouwer (1996), Monitoring space weather with the GOES magnetometers, *Proc. SPIE*, *2812*, 299–308.
Slinker, S. P., J. A. Fedder, J. Chen, and J. G. Lyon (1998), Global MHD simulation of the magnetosphere and ionosphere for 1930–2330 UT on November 3, 1993, *J. Geophys. Res.*, *103*(A11), 26,243–26,250, doi:10.1029/97JA02775.
Snekvik, K., et al. (2007), Cluster observations of a field aligned current at the dawn flank of a bursty bulk flow, *Ann. Geophys.*, *25*, 1405–1415, doi:10.5194/angeo-25-1405-2007.
Stenbaek-Nielsen, H. C., and A. Otto (1997), Conjugate auroras and the interplanetary magnetic field, *J. Geophys. Res.*, *102*(A2), 2223–2232, doi:10.1029/96JA03563.
Tenfjord, P., and N. Østgaard (2013), Energy transfer and flow in the solar wind-magnetosphere-ionosphere system: A new coupling function, *J. Geophys. Res. Space Physics*, *118*, 5659–5672, doi:10.1002/jgra.50545.

Tenfjord, P., N. Østgaard, K. Snekvik, K. M. Laundal, J. P. Reistad, S. Haaland, and S. E. Milan (2015), How the IMF B_y induces a B_y component in the closed magnetosphere and how it leads to asymmetric currents and convection patterns in the two hemispheres, *J. Geophys. Res. Space Physics*, *120*, 9368–9384, doi:10.1002/2015JA021579.
Tsyganenko, N. A. (2002), A model of the near magnetosphere with a dawn-dusk asymmetry, *J. Geophys. Res.*, *107*(A8), 1–17, doi:10.1029/2001JA000219.
Tsyganenko, N. A., and D. H. Fairfield (2004), Global shape of the magnetotail current sheet as derived from Geotail and Polar data, *J. Geophys. Res.*, *109*, 1–11, doi:10.1029/2003JA010062.
Walker, R. J., R. L. Richard, T. Ogino, and M. Ashour-Abdalla (1999), The response of the magnetotail to changes in the IMF orientation: The magnetotail's long memory, *Phys. Chem. Earth Part C*, *24*(l), 221–227, doi:10.1016/S1464-1917(98)00032-4.
Weimer, D. R., and J. H. King (2008), Improved calculations of interplanetary magnetic field phase front angles and propagation time delays, *J. Geophys. Res.*, *113*, 1–14, doi:10.1029/2007JA012452.
Wing, S., P. T. Newell, D. G. Sibeck, and K. B. Baker (1995), A large statistical study of the entry of interplanetary magnetic field Y-component into the magnetosphere, *Geophys. Res. Lett.*, *22*(16), 2083–2086, doi:10.1029/95GL02261.
Wing, S., D. G. Sibeck, M. Wiltberger, and H. Singer (2002), Geosynchronous magnetic field temporal response to solar wind and IMF variations, *J. Geophys. Res.*, *107*(A8), 1–10, doi:10.1029/2001JA009156.
Yu, Y., and A. J. Ridley (2009), Response of the magnetosphere-ionosphere system to a sudden southward turning of interplanetary magnetic field, *J. Geophys. Res.*, *114*, A03216, doi:10.1029/2008JA013292.